

Using CaCO₃-doped package to improve correlated color temperature uniformity of white light-emitting diodes

My Hanh Nguyen Thi¹, Nguyen Thi Phuong Loan², Thuc Minh Bui³, Hoang Van Ngoc⁴

¹Faculty of Mechanical Engineering, Industrial University of Ho Chi Minh City, Vietnam

²Faculty of Fundamental 2, Posts and Telecommunications Institute of Technology, Vietnam

³Faculty of Electrical and Electronics Engineering, Nha Trang University, Vietnam

⁴Institute of Applied Technology, Thu Dau Mot University, Vietnam

Article Info

Article history:

Received Sep 9, 2020

Revised Apr 29, 2021

Accepted Jun 12, 2021

Keywords:

CaCO₃

Color quality scale

Luminous flux

Mie-scattering theory

WLEDs

ABSTRACT

The white light-emitting diode (WLED) has been the most advance lighting method currently, however, the fabrication process of this configuration still has drawbacks which negatively affect its color quality. This research was conducted to provide a method for WLED's lighting output enhancement. Since CaCO₃ particles are excellent for thermal stability enhancement, especially when being combined with an adhesive substance, we decided to integrate CO₃ particles into resin matrix such as melamine formaldehyde (MF) and investigate their influences on the optical properties, including color uniformity and lumen output, of the WLED. The results showed that CaCO₃ and MF resin are beneficial to the light scattering efficiency, which results in higher luminous flux and chromatic quality for WLED packages. In addition to that, the appropriate amounts of MF resin and CaCO₃ for reaching the best lumen efficiency and color quality are figured out at 1% and 10%, respectively. Moreover, another advantage of using MF resin and CaCO₃ for fabricating WLEDs is cost effectiveness. Hence, it has turned out that CaCO₃ and MF resins can be potential materials for next high-quality WLED generations.

This is an open access article under the [CC BY-SA](https://creativecommons.org/licenses/by-sa/4.0/) license.



Corresponding Author:

Hoang Van Ngoc

Institute of Applied Technology

Thu Dau Mot University

No 6, Tran Van On Street, Thu Dau Mot city, Binh Duong province, Vietnam

Email: ngochv@tdmu.edu.vn

1. INTRODUCTION

The effectiveness of using encapsulation added with scattering particles for boosting the performance of white light-emitting diode (WLED) structures has been recognized by many researchers. The application of diffuser-doped encapsulation promotes the lighting efficiency of lighting devices while increasing other aspects of scattered light to result in better color quality. Although high refractive index is an advantage that diffuser-loaded encapsulation offers, the excessive index of refraction induces issues in scattering process. In particular, the materials with high refractive index are favored in WLED production because it can effectively improve the lighting performance of the devices. Nevertheless, the light loss resulted from the internal reflection is the main problem that prevent them from being widely used in WLED fabrication. In the WLED using GaN base, the discrepancy of refractive indices between GaN and the opposing surface leads to the generated light being stuck inside the side having higher refractive index. In particular, the existing path for extracted light in GaN is located at 23.50°, which leads to the chance of only 4% energy transmitted through [1], [2]. In another encapsulation with AlGaInP semiconductor that also has

poor light converting rate, this angle is 17° . These are evidences for the importance of appropriate refractive indices in controlling lighting efficiency and minimizing unnecessary light loss. Many efforts were made to eradicate or at least limit the light loss from photon entrapment and reabsorption. Some research papers suggested reorganizing the LED configuration [3], [4], others tried to modify the contacting area [5], [6], yet a practical and reliable solution to address the refractive index discrepancy problem has not been found. Lee *et al.* pioneered employing multiple materials with distinct refractive indices to create an innovative encapsulation package with low impact from refractive index contrast [7].

The organization of this package is the light-transmitting chips at the bottom, and above them are other layers whose refractive indexes are arranged from the highest to the lowest. The addition of resin and CaCO_3 particles stimulated the scattering events, resulting in the variation of light transmission course and consistency in far-field. Therefore, we can obtain the light that was lost due to excessive refractive index when using this configuration. In other cases of the configuration emitting several colors, the resin combined diffusional particles supported the homogeneity of extracted color. The resin-diffuser combination can be translucent under light or non-transparent in cases of BaSO_4 , TiO_2 , CaF_2 , and SiO_2 , which also exhibited distinct refractive index from the package [8]. In another research of Lester *et al.* the idea of using microscopic molecule of Titania, Magnesia, Yttria, Zirconia, Alumina, GaN, AlN, ZnO, and ZnSe was proposed as a solution for high refractive substance [9]. However, the problem arose when the microscopic molecule bounded to a structure cannot radiate under uniform distribution or when the discrepancy between the molecule and emission frequency is large. The report of Gu *et al.* claimed that submerging method on InGaN quantum wells (QWs) of lighting device when deploying the 520 nm TiO_2 increased the light output by 85% [10]. TiO_2 and GaN are also compatible in terms of refractive index and translucent domain. However, the issue is the refractive index of TiO_2 doped package is too high and would lead to a substantial refractive-index discrepancy at the contacting surface of package outer layer and the environment. The organic silicon compound and polymethylmethacrylate which have the same refractive index are not sufficient because the organic silicon has low scattering capacity, and polymethylmethacrylate cannot excel under high heat. Low chromatic quality is another problem that phosphor-converted WLED is facing.

The reason is due to the uneven distribution of phosphor particles on the surface of lighting chip causing a mismatch between the light discharging model of LED chips and the density of phosphor particles. As a result, the unevenly coated phosphor layer cannot fully enhance light emission of LED chips. Many intensive researches were conducted and proposed numerous effective methods such as conformal coating method, electrophoretic deposition, vaporizing the solvent and phosphor, and adding a layer of luminous ceramic to improve color deviation minimization, phosphor packaging, and distribution of angular color temperature [11]-[14]. However, the imbalance between the proportions of blue and yellow lights at different angles in the package that leads to a low color quality has not been thoroughly solved since there was no mention of angular color uniformity on the researches above [15]. The adjustment of blue and yellow lights is often discussed as the yellow light adapted to the blue light [16], while in fact, the blue light, after being discharged, does not immediately reach the outer layer but interacts with the phosphor setup and light diversion events such as light transmission, absorption, and reflection.

The property of light absorbed by phosphor particles determines Stoke's Shift and emission spectrum, therefore, phosphor particle is suitable to be a scattering enhancing material. With sub micrometer-micrometer size phosphor particles, the amount of emitted light depends on Mie-scattering. However, considering the effect of phosphor material on the better angular color homogeneity, the phosphor particles can be solely utilized for the chromatic quality purpose, while becoming a scattering enhancer can be regarded as a side function [17]. Kim *et al.* claimed that using microscopic particles of silicone resin that are injected to the package in the form of fluid can enhance WLED color quality [18]. Chen *et al.* suggested managing color temperature deviation at -70° to 70° directions with a compound of nanoscopic ZrO_2 particles and silicone resin, leading to an effective chromatic deviation reduction from 1000 to 420 K [19]. Nonetheless, to continue working on the color enhancement, we studied and introduced another modified package that is less complicated but still able to optimize the correlated color temperature. As the problems has been presented, using the composite as an encapsulation with adequate refractive indexes such as melamine formaldehyde (MF) resin and CaCO_3 are appropriate to be fused into lighting materials and studied for optical development. In addition to that, among the scattering enhancement particles, CaCO_3 is the one can perform better color homogeneity and high lumen efficiency simultaneously [20]. CaCO_3 has also been combined with other organic resin such as epoxy resin to enhance the thermal stability and the mechanical strength [21].

In this study, the effect of MF resin and CaCO_3 with different concentrations will be investigated. To start the investigation, the simulation of a WLED utilizing CaCO_3 and MF resin is built and the scattering calculation based on Mie-scattering theory is displayed, as shown in section 2. The experimental results are discussed and explained in section 3, and finally summarized in section 4.

2. RESEARCH METHOD

2.1. MC-WLEDs simulation

Two common approaches applied to modify a substance's refractive index are the fabrication and the combining methods. In fabrication method, the materials with adequate refractive index, usually the polymer with group of high refraction atoms such as benzene and halogen, are generated by organic-compound integration. The combining method utilizes an existing material with high refractive capability and coats it evenly on the package to achieve suitable refractive index. The material particles used in combining method must get its shape modified to expand surface and minimize thickness. Such changes are beneficial to particles at microscopic size, making it easier for them to bind to each other and elevate light scattering capacity.

The simulated WLEDs in this research applied the combining method with the approach based on Mont *et al.* [22]. Precautionary measures are applied to achieve optimal results, for example, the compound is coated with toluene, after the drying stage, using magnetic stirrer to prevent pervasion of impure substances and water. Likewise, surfactant is applied to the compound of 2h thickness through reflux method at a suitable volume. The surfactant prevents the particles from merging by lessening the attractive force between particles and results in an enhanced scattering property. The adjusted MF/CaCO₃ compound after the shape reformation is placed into the ultrasonic cleaner to add Dow Corning 6550 gel for 5 minutes before being applied on the lighting configuration. Figure 1 provides a specific illustration of the WLED model in the research. The realistic setup is shown in Figure 1(a) and technical details of the components are in Figure 1(b). Figure 1(c) is the image of WLEDs simulation using the Monte Carlo ray tracing on the optical engineering program LightTools 8.1.0. The WLED configuration consists of reflectors, LED chips, phosphor layer, and a half-sphere glass cover. The reflectors are 8 x 2.07 x 9.85 mm in the bottom, side, and top, respectively. 9 LED chips are bound to the holes within the reflectors, and their measurement is 0.15 mm in height, 1.14 mm² in size, and 1.16 W energy emission at peak wavelength of 453 nm. Above the chip is a 0.08 mm thick phosphor layer containing phosphor particles with a value of 14.5 μm in average diameter. After GaN-based LED chips are wire bonded on the lead frame, they are coated with the mixture of 6550 silicone gel with 10% wt. YAG:Ce³⁺ yellow phosphor. The package is then going through a heat treatment process at 120 °C for 30 minutes to have it fixed. Next, the LED lens is attached to the frame and the encapsulation of MF resin and CaCO₃ particles is subsequently filled into the gap between the lens and chips. Then, the package filled with MF/CaCO₃ is baked at 150°C for an hour to complete the experimented simulation.

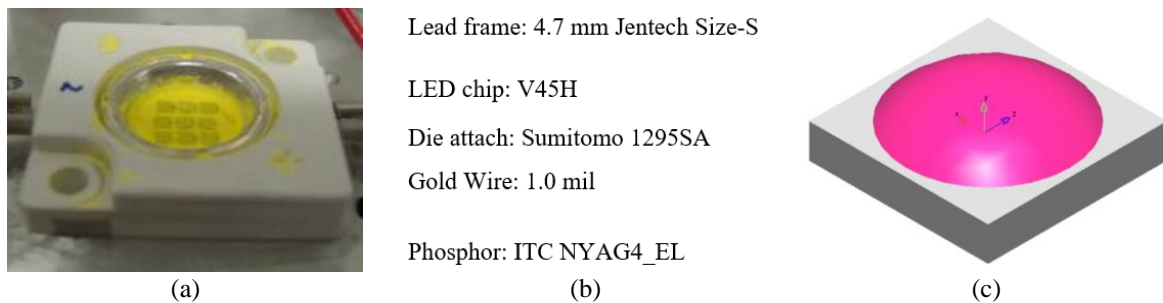


Figure 1. Illustration of phosphor-converted MCW-LEDs as doping CaCO₃: (a) the actual MCW-LEDs, (b) its parameters and (c) simulation of MCW-LEDs

2.2. Scattering computation

The purpose of this part is to demonstrate the computing procedure to determine resultant optical properties. The mathematical models applied in the computing procedure are developed based on Mie-theory and Monte Carlo method because these scientific theories are the functioning core of optical engineering programs such as Lighttools, Tracepro, and ASAP [23]-[26]. It is more reliable and even possible to acquire an improvement in structure and simulation process when using these modified mathematical models to calculate the optical properties of lighting configuration. According to Mie-theory, scattering coefficient $\mu_{sca}(\lambda)$, anisotropy factor $g(\lambda)$, and reduced scattering coefficient $\delta_{sca}(\lambda)$ are calculated via [27]-[30]:

$$\mu_{sca}(\lambda) = \int N(r) C_{sca}(\lambda, r) dr \quad (1)$$

$$g(\lambda) = 2\pi \int \int_{-1}^1 p(\theta, \lambda, r) f(r) \cos\theta d \cos\theta dr \quad (2)$$

$$\delta_{sca} = \mu_{sca}(1 - g) \quad (3)$$

where, $N(r)$ represents the amount of scattering particles (per mm^3). C_{sca} is the scattering cross section (mm^2). λ (nm) expresses the wavelength of incident light, and r (mm) represents the diameter of phosphor particles. θ indicates the degree in which the scattering event happens. $p(\theta, \lambda, r)$ is the phase function, and $f(r)$ is the function for SEP size distribution in phosphor film. Both $f(r)$ and $p(\theta, \lambda, r)$ can be determined using:

$$f(r) = f_{dif}(r) + f_{phos}(r) \quad (4)$$

$$\begin{aligned} N(r) &= N_{dif}(r) + N_{phos}(r) \\ &= K_N \cdot [f_{dif}(r) + f_{phos}(r)] \end{aligned} \quad (5)$$

$N_{dif}(r)$ and $N_{phos}(r)$ are numbers of diffusor and phosphor particles in the scattering layer. $f_{dif}(r)$ and $f_{phos}(r)$ are functions of diffusor and phosphor particle the size distribution. The amount of diffusional particles $M(r)$ in 1% concentration is K_N and can be defined from the diffusor mass distribution equation below:

$$c = K_N \int M(r) dr \quad (6)$$

$$M(r) \frac{4}{3} \pi r^3 [\rho_{dif} f_{dif}(r) + \rho_{phos} f_{phos}(r)] \quad (7)$$

where $\rho_{dif}(r)$ is the amount of diffusional particles, and $\rho_{phos}(r)$ is the amount of phosphor particles. The scattering coefficient (C_{sca}) is the result of the following expression based on Mie scattering:

$$C_{sca} = \frac{2\pi}{k^2} \sum_0^{\infty} (2n-1)(|a_n|^2 + |b_n|^2) \quad (8)$$

The value of $k = 2\pi/\lambda$, while a_n and b_n are estimated from:

$$\alpha_n(x, m) = \frac{\psi_n(mx)\psi_n(x) - m\psi_n(mx)\psi_n(x)}{\psi_n(mx)\xi_n(x) - m\psi_n(mx)\xi_n(x)} \quad (9)$$

$$b_n(x, m) = \frac{m\psi_n(mx)\psi_n(x) - \psi_n(mx)\psi_n(x)}{m\psi_n(mx)\xi_n(x) - \psi_n(mx)\xi_n(x)} \quad (10)$$

In (9) and (10), x is the result of k multiplies by r , index of refraction is expressed as m , while $\psi_n(x)$ and $\xi_n(x)$ are the Riccati-Bessel function. This allows m_{dif} and m_{phos} , the relative refractive index of diffusor and phosphor particles, to be resolved from $m_{dif} = n_{dif}/n_{sil}$ and $m_{phos} = n_{phos}/n_{sil}$, which completes the phase function as:

$$\rho(\theta, \lambda, r) = \frac{4\pi\beta(\theta, \lambda, r)}{k^2 C_{sca}(\lambda, r)} \quad (11)$$

with $\beta(\theta, \lambda, r)$ and the angular scattering amplitudes $S_1(\theta)$ and $S_2(\theta)$ yielded from:

$$\beta(\theta, \lambda, r) = \frac{1}{2} [|S_1(\theta)|^2 + |S_2(\theta)|^2] \quad (12)$$

$$S_1 = \sum_{n=1}^{\infty} \frac{2n+1}{n(n+1)} \left[\alpha_n(x, m)\tau_n(\cos\theta) + b_n(x, m)\tau_n(\cos\theta) \right] \quad (13)$$

$$S_2 = \sum_{n=1}^{\infty} \frac{2n+1}{n(n+1)} \left[\alpha_n(x, m)\tau_n(\cos\theta) + b_n(x, m)\tau_n(\cos\theta) \right] \quad (14)$$

The lighting characteristics of yttrium aluminum garnet doped with cerium (CE) is the research subject of many studies, however, the changes in α depends on the amount of CE, the synthesis method, and estimate devices. With cerium doped YAG, it is possible for α to exceed 15 mm^{-1} and the radiation intake to be improved considerably in comparison to the standard array of $3-8 \text{ mm}^{-1}$ for α in blue radiation. This is because the particles of YAG:Ce are microscopic, which promotes inner reflection and enhances the total

light absorption. To investigate the fluctuation of C_{sca} (453) in blue light, we setup an α that varies in the range from 8 to 20 mm^{-1} and a phosphor crystalline material with high α . The scattering cross section of CaCO_3 in connection with the emission wavelength is presented in Figure 2. The scattering cross section in Figure 2 is higher than the absorption, which suggests that high C_{sca} of CaCO_3 phosphor particles can lead to better absorption ability.

The scattering coefficient measured from (1) is presented in Figure 3. Analyzing the results of Figure 3, we can see that CaCO_3 phosphor particles benefits the growth of scattering and absorption coefficients. This showed that increasing the CaCO_3 concentration in the package is an effective method to optimize the chromatic performance. Figure 4 expressed the reduction of scattering coefficient in package with CaCO_3 . The results of (3) presented in Figure 4 and the contents of Figure 2 can be used to evaluate the performance of Mie-scattering and Monte Carlo method. According to Figures 2 and 4, the scattering coefficient and scattering coefficient reduction of the ray-tracing method are higher than Mie-scattering. The results of μ_{abs} (453 nm) measured by ray-tracing is usually 1.63 while Mie-scattering's result is at 1.47.

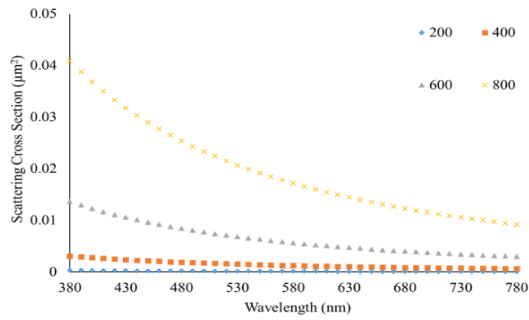


Figure 2. The scattering cross sections of CaCO_3 particles

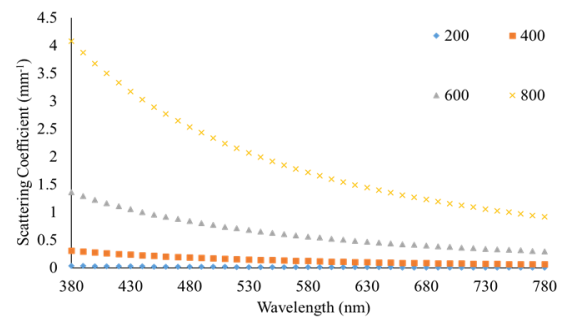


Figure 3. Scattering coefficients of CaCO_3 particles

The resultant blue and yellow lights achieved from a lighting device are usually estimated by using a model based on Lambert's law. The schott BK7 glass is applied as projecting ocular and supporting structure. The white material with absorption and scattering ratio of 11.1:89.9 is distributed on the interior side of the spheres. The integrating spheres with diffused white reflective coating inner are tools to capture transmitted or reflected radiation. The model of WLEDs uses Monte Carlo ray-tracing as a solution to integrate the amount of light collected. Because the nature of phosphor particles is Mie-scattering, and Monte Carlo ray-tracing is ineffective in determining the diffusing angles of phosphor, the estimation of angular distribution of light intensity is carried out using the Henyey-Greenstein function. The phase function of CaCO_3 particles was calculated and presented in Figure 5. Based on the comparison between these two methods, the results demonstrated that the effects of Mie scattering were insignificant on the lighting performance. Meanwhile, the ray-tracing presented significant results on optical properties, for example lower blue light absorption and higher light transmission. These changes were concluded when two methods were compared to the original measurements, from which the scattering and absorption coefficient were lower, and the anisotropy factor was higher than the correct number. Therefore, to ensure the measurement accuracy, we modified two out of three constants and retained one throughout the experiment process.

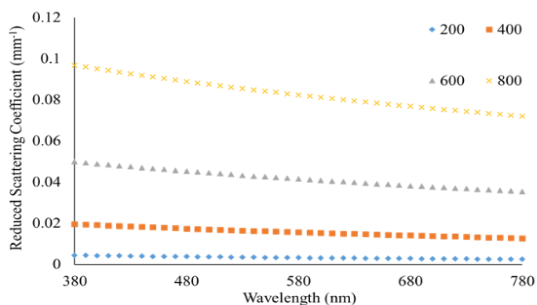


Figure 4. The reduced scattering coefficient of CaCO_3 particles

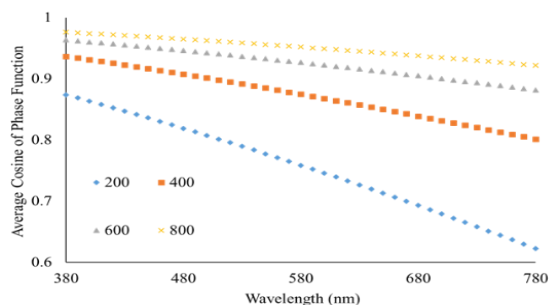


Figure 5. The phase function of CaCO_3 particles

3. RESULTS AND DISCUSSION

In Figure 6 is the angular CCT distribution of WLED package with CaCO_3 . The angular CCT distributions of the diffuser-loaded package and LED chip light are identical and can be concluded as Lambertian pattern. The phosphor layer emits a blue light at the source that gradually turns yellow toward the verge. As the angular CCT distribution is not compatible with density angular distribution, the side angles, -90° or 90° , of lighting chips shows insufficient CCT, while 0° CCT at the center is better. The enhancement of angular CCT distribution would raise the highest and lowest thresholds of CCT. The spatial variability of CCT can also be managed with diffuser-filled package, specifically MF resin diffuser showed less spatial CCT deviation than CaCO_3 with the same amount. This is because the nature of CaCO_3 particles is different from that of MF resin, in other words, the bigger particle size of CaCO_3 makes it induce the deviation of spatial CCT. Figure 7 presents the light output results of WLED configurations using CaCO_3 . According to these results, it seems that as the concentration of CaCO_3 rises, the angular CCT deviation decreases. This is a positive effect for color performance management, although the diffuser particles also have a negative influence on lumen output. In terms of CCT deviation reduction, the MF resin also has a great contribution since the deviation of angular-dependent color temperature in the package with MF resin is always lower than in the one without MF resin. When being used at the same concentration with that of CaCO_3 particle, the scattering ability of MF resin can impact color deviation and reduce it by 1.5 time, while the deviation reduction of CaCO_3 with different scattering properties would barely reach 0.7. However, the CaCO_3 particles provide better management over the reduction of lumen output than MF resin, which benefits the luminous efficiency. Thus, it is essential to choose the appropriate amounts of CaCO_3 and MF resin to achieved the best optical performances for WLED devices.

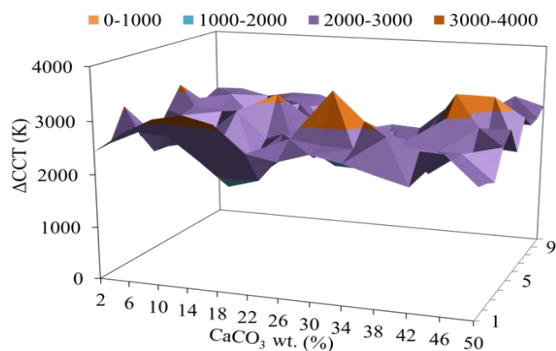


Figure 6. The ΔCCT of LED packaging with CaCO_3 particles

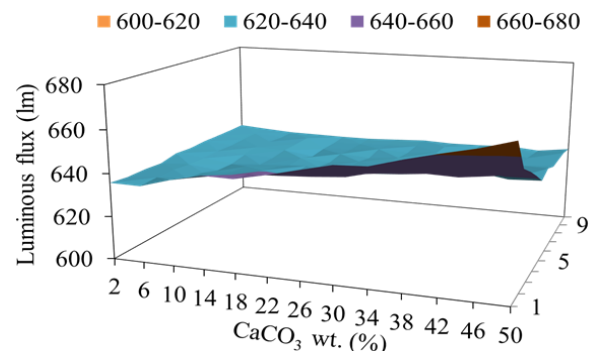


Figure 7. The luminous flux of LED packaging with CaCO_3 particles

Particularly, the light loss from absorption caused by 10% CaCO_3 is lower than the one resulted from 1% MF. So, WLED package with MF resin diffuser would have the color deviation reduced by 1.5, on the other hand, CaCO_3 -doped package would have 0.7 deviation reduction while retaining a lower light loss than the MF package. At similar mass, the MF resin diffuser and CaCO_3 diffuser demonstrate different parameters in density distribution, particle size, scattering coefficient, and particles number. MF resin has higher particle density than CaCO_3 because the particle size of MF is $3\ \mu\text{m}$ while $15\ \mu\text{m}$ is the size of CaCO_3 particle, which means MF has better scattering efficiency. Although stronger light scattering is more advantageous to color quality, it would prevent the transmission of light and damage the light output. As a result, the value of scattering and transmitted light should be equal to maintain good results in both color temperature consistency and lighting capacity.

4. CONCLUSION

With the attempt to prove the effectiveness of CaCO_3 and MF compound in accomplishing the lighting properties' improvement of the LED lighting devices, the research has conducted many experiments with the packages containing CaCO_3 particles and MF resin. The simulation of WLED packages in this study is built using combining method based on Mont *et al.* The Mie-scattering theory and Lambert-Beer law are applied to form the mathematic computation for analyzing and verifying the obtained results. The addition of MF resin and CaCO_3 particles significantly enhances the scattering ability of lights inside WLED package, resulting in higher color uniformity. However, the MF resin and CaCO_3 should be used with the proper

amount to optimize the lumen output of WLED. Specifically, if the concentration of MF resin is more than 1%, the lumen output will decrease significantly due to the excessive scattering events. Meanwhile, 10% CaCO₃ is the most suitable content since this amount can result in both higher lumen output and better chromatic homogeneity. This research has proposed a promising approach to the improvement of WLEDs' light performances. This, moreover, can be applied in manufacturing WLED packages or used as reference for further studies.

ACKNOWLEDGEMENTS

This research is supported by Industrial University of Ho Chi Minh City (IUH) under grant number 112/HD-DHCN.

REFERENCES

- [1] C. Zhang, L. Xiao, P. Zhong, and G. He, "Photometric optimization and comparison of hybrid white LEDs for mesopic road lighting," *Applied Optics*, vol. 57, no. 16, pp. 4665-4671, 2018, doi: 10.1364/AO.57.004665.
- [2] S. J. Dain, D. A. Atchison, J. K. Hovis, and M.-Y. Boon, "Lighting for color vision examination in the era of LEDs: the FM100Hue Test," *Journal of the Optical Society of America A*, vol. 37, no. 4, pp. A122-A132, 2020, doi: 10.1364/JOSAA.382301.
- [3] G. Xia, Y. Ma, X. Chen, S. Q. Jin, and C. Huang, "Comparison of MAP method with classical methods for bandpass correction of white LED spectra," *Journal of the Optical Society of America A*, vol. 36, no. 5, pp. 751-758, 2019, doi: 10.1364/JOSAA.36.000751.
- [4] S. Rasouli, S. Hamzeloui, and D. Hebri, "Colorful radial Talbot carpet at the transverse plane," *Optics Express*, vol. 27, no. 13, pp. 17435-17448, 2019, doi: 10.1364/OE.27.017435.
- [5] H. L. Ke *et al.*, "Lumen degradation analysis of LED lamps based on the subsystem isolation method," *Applied Optics*, vol. 57, no. 4, pp. 849-854, 2018, doi: 10.1364/AO.57.000849.
- [6] D. Lu *et al.*, "Synthesis and photoluminescence characteristics of the LiGd₃MoO₄·5Eu³⁺ red phosphor with high color purity and brightness," *Optical Materials Express*, vol. 8, no. 2, pp. 259-269, 2018, doi: 10.1364/OME.8.000259.
- [7] B. Qiu, K. Li, and X. Li, "Synthesis and enhanced luminescent properties of SiO₂@LaPO₄:Ce³⁺/Tb³⁺ microspheres," *Optical Materials Express*, vol. 8, no. 1, pp. 59-65, 2018, doi: 10.1364/OME.8.000059.
- [8] Y. P. Chang *et al.*, "New scheme of LiDAR-embedded smart laser headlight for autonomous vehicles," *Optics Express*, vol. 27, no. 20, pp. A1481-A1489, 2019, doi: 10.1364/OE.27.0A1481.
- [9] H. Gu, M. Chen, Qixia Wang, and Qi. Tan, "Design of two-dimensional diffractive optical elements for beam shaping of multicolor light-emitting diodes," *Applied Optics*, vol. 57, no. 10, pp. 2653-2658, 2018, doi: 10.1364/AO.57.002653.
- [10] C. Tian *et al.*, "Mn⁴⁺ activated Al₂O₃ red-emitting ceramic phosphor with excellent thermal conductivity," *Optics Express*, vol. 27, no. 22, pp. 32666-32678, 2019, doi: 10.1364/OE.27.032666.
- [11] X. Yuan *et al.*, "Ultra-high capacity for three-dimensional optical data storage inside transparent fluorescent tape," *Optics Letters*, vol. 45, no. 6, pp. 1535-1538, 2020, doi: 10.1364/OL.387278.
- [12] L. V. Labunets, A. B. Borzov, and I. M. Akhmetov, "Regularized parametric model of the angular distribution of the brightness factor of a rough surface," *Journal of Optical Technology*, vol. 86, no. 10, pp. 618-626, 2019, doi: 10.1364/JOT.86.000618.
- [13] A. D. Corbett *et al.*, "Microscope calibration using laser written fluorescence," *Optics Express*, vol. 26, no. 17, pp. 21887-21899, 2018, doi: 10.1364/OE.26.021887.
- [14] Z. Song, T. Guo, X. Fu, and X. Hu, "Residual vibration control based on a global search method in a high-speed white light scanning interferometer," *Applied Optics*, vol. 57, no. 13, pp. 3415-3422, 2018, doi: 10.1364/AO.57.003415.
- [15] X. Leng *et al.*, "Feasibility of co-registered ultrasound and acoustic-resolution photoacoustic imaging of human colorectal cancer," *Biomedical Optics Express*, vol. 9, no. 11, pp. 5159-5172, 2018, doi: 10.1364/BOE.9.005159.
- [16] F. Guan, G. Jiang, Y. Song, M. Yu, Z. Peng, and F. Chen, "No-reference high-dynamic-range image quality assessment based on tensor decomposition and manifold learning," *Applied Optics*, vol. 57, no. 4, pp. 839-848, 2018, doi: 10.1364/AO.57.000839.
- [17] X. Huang *et al.*, "Effect of electron-transfer quenching on the photoluminescence of Pr³⁺ in MgXO₃, X = Ge, Si," *Optical Materials Express*, vol. 10, no. 5, pp. 1163-1168, 2020, doi: 10.1364/OME.389599.
- [18] J. J. Gómez-Valverde *et al.*, "Automatic glaucoma classification using color fundus images based on convolutional neural networks and transfer learning," *Biomedical Optics Express*, vol. 10, no. 2, pp. 892-913, 2019, doi: 10.1364/BOE.10.000892.
- [19] X. Ding *et al.*, "Improving the optical performance of multi-chip LEDs by using patterned phosphor configurations," *Optics Express*, vol. 26, no. 6, pp. A283-A292, 2018, doi: 10.1364/OE.26.00A283.
- [20] L. M. Lozano *et al.*, "Optical engineering of polymer materials and composites for simultaneous color and thermal management," *Optical Materials Express*, vol. 9, no. 5, pp. 1990-2005, 2019, doi: 10.1364/OME.9.001990.
- [21] S. Beldi *et al.*, "High Q-factor near infrared and visible Al₂O₃-based parallel-plate capacitor kinetic inductance detectors," *Optics Express*, vol. 27, no. 9, pp. 13319-13328, 2019, doi: 10.1364/OE.27.013319.

- [22] Y. Chu *et al.*, "Perception enhancement using importance-driven hybrid rendering for augmented reality based endoscopic surgical navigation," *Biomedical Optics Express*, vol. 9, no. 11, pp. 5205-5226, 2018, doi: 10.1364/BOE.9.005205.
- [23] H. Y. Yu *et al.*, "Solar spectrum matching with white OLED and monochromatic LEDs," *Applied Optics*, vol. 57, no. 10, pp. 2659-2666, 2018, doi: 10.1364/AO.57.002659.
- [24] S. Feng, and Jigang Wu, "Color lensless in-line holographic microscope with sunlight illumination for weakly-scattered amplitude objects," *OSA Continuum*, vol. 2, no. 1, pp. 9-16, 2019, doi: 10.1364/OSAC.2.000009.
- [25] R. O'Shea, S. R. Laney, and Z. Lee, "Evaluation of glint correction approaches for fine-scale ocean color measurements by lightweight hyperspectral imaging spectrometers," *Applied Optics*, vol. 59, no. 7, pp. B18-B34, 2020, doi: 10.1364/AO.377059.
- [26] Y. Li *et al.*, "395 nm GaN-based near-ultraviolet light-emitting diodes on Si substrates with a high wall-plug efficiency of 52.0% @350 mA," *Optics Express*, vol. 27, no. 5, pp. 7447-7457, 2019, doi: 10.1364/OE.27.007447.
- [27] N. Anous, T. Ramadan, M. Abdallah, K. Qaraq, and D. Khalil, "Impact of blue filtering on effective modulation bandwidth and wide-angle operation in white LED-based VLC systems," *OSA Continuum*, vol. 1, no. 3, pp. 910-929, 2018, doi: 10.1364/OSAC.1.000910.
- [28] A. Motazedifard, S. Dehbod, and A. Salehpour, "Measurement of thickness of thin film by fitting to the intensity profile of Fresnel diffraction from a nanophase step," *Journal of the Optical Society of America A*, vol. 35, no. 12, pp. 2010-2019, 2018, doi: 10.1364/JOSAA.35.002010.
- [29] H. S. Ghoroury, Y. Nakajima, M. Yeh, E. Liang, C.-Li Chuang, and J. C. Chen, "Color temperature tunable white light based on monolithic color-tunable light emitting diodes," *Optics Express*, vol. 28, no. 2, pp. 1206-1215, 2020, doi: 10.1364/OE.375320.
- [30] T. Bui, R. Cusani, G. Scarano, and M. Biagi, "Metameric MIMO-OOK transmission scheme using multiple RGB LEDs," *Optics Express*, vol. 26, no. 11, pp. 14038-14050, 2018, doi: 10.1364/OE.26.014038.